FULL PAPER

Reproducibility of ¹⁹F-MR ventilation imaging in healthy volunteers

Benjamin J. Pippard[1,2] | Mary A. Neal[1,2] (iD) | Adam M. Maunder[3] (iD) |
Kieren G. Hollingsworth[1,2] | Alberto Biancardi[3] | Rod A. Lawson[4] | Holly Fisher[5] |
John N. S. Matthews[5,6] | A. John Simpson[2,7] (iD) | Jim M. Wild[3] (iD) | Peter E. Thelwall[1,2] (iD)

[1]Newcastle Magnetic Resonance Centre, Newcastle University, Newcastle upon Tyne, United Kingdom

[2]Translational and Clinical Research Institute, Newcastle University, Newcastle upon Tyne, United Kingdom

[3]POLARIS, Department of IICD, University of Sheffield, Royal Hallamshire Hospital, Sheffield, United Kingdom

[4]Respiratory Medicine, Sheffield Teaching Hospitals National Health Service Foundation Trust, Sheffield, United Kingdom

[5]Population Health Sciences Institute, Newcastle University, Newcastle upon Tyne, United Kingdom

[6]School of Mathematics, Statistics and Physics, Newcastle University, Newcastle upon Tyne, United Kingdom

[7]Respiratory Medicine, Newcastle upon Tyne Hospitals National Health Service Foundation Trust, Newcastle upon Tyne, United Kingdom

Correspondence
Peter E. Thelwall, Newcastle Magnetic Resonance Centre, Campus for Ageing and Vitality, Newcastle University, Newcastle upon Tyne, NE4 5PL, United Kingdom.
Email: pete.thelwall@newcastle.ac.uk

Funding information
Medical Research Council Developmental Pathways Funding Scheme award (MR/N018915/1) to PT and a Medical Research Council Capital Research Infrastructure award (MR/M008894/1) to JW

Purpose: To assess the reproducibility of percentage ventilated lung volume (%VV) measurements in healthy volunteers acquired by fluorine (¹⁹F)-MRI of inhaled perfluoropropane, implemented at two research sites.

Methods: In this prospective, ethically approved study, 40 healthy participants were recruited (May 2018-June 2019) to one of two research sites. Participants underwent a single MRI scan session on a 3T scanner, involving periodic inhalation of a 79% perfluoropropane/21% oxygen gas mixture. Each gas inhalation session lasted about 30 seconds, consisting of three deep breaths of gas followed by a breath-hold. Four ¹⁹F-MR ventilation images were acquired per participant, each separated by approximately 6 minutes. The value of %VV was determined by registering separately acquired ¹H images to ventilation images before semi-automated image segmentation, performed independently by two observers. Reproducibility of %VV measurements was assessed by components of variance, intraclass correlation coefficients, coefficients of variation (CoV), and the Dice similarity coefficient.

Results: The MRI scans were well tolerated throughout, with no adverse events. There was a high degree of consistency in %VV measurements for each participant ($CoV_{observer1} = 0.43\%$; $CoV_{observer2} = 0.63\%$), with overall precision of %VV measurements determined to be within ± 1.7% (95% confidence interval). Interobserver agreement in %VV measurements revealed a high mean Dice similarity coefficient (SD) of 0.97 (0.02), with only minor discrepancies between observers.

Benjamin J. Pippard and Mary A. Neal contributed equally to this work.

Conclusion: We demonstrate good reproducibility of %VV measurements in a group of healthy participants using ^{19}F-MRI of inhaled perfluoropropane. Our methods have been successfully implemented across two different study sites, supporting the feasibility of performing larger multicenter clinical studies.

1 | INTRODUCTION

Magnetic resonance imaging is an attractive approach to the investigation of respiratory disease, given its noninvasive nature and lack of exposure to ionizing radiation. Conventional MRI of the lungs remains challenging, however, due primarily to the low proton density of lung tissue and magnetic field inhomogeneities that exist at ubiquitous air–tissue interfaces.[1] The use of exogenous gas agents can overcome these challenges by direct visualization of inhaled gas within the lungs, enabling assessment of regional ventilation properties. Specifically, hyperpolarized-gas MRI (HP-MRI) is well established in research settings[2,3] and has led to the development of novel imaging biomarkers relating to lung function.[4-6] Of these, the percentage ventilated lung volume (%VV) and related ventilation defect percentage have been reported widely,[7,8] providing clinically useful metrics of ventilatory function that correlate strongly with conventional spirometric indices.[9,10] Previous studies have established the reproducibility of these HP-MRI measurements in healthy volunteers[7,9,11] and patients with respiratory disease,[11-14] showing improved sensitivity to early smoking-related disease[15] and asthma control[16] compared with spirometry. However, the requirement for specialized polarizing equipment and expertise remains a potential barrier to widespread clinical adoption of this technique.

The ^{19}F-MRI of inhaled perfluoropropane (PFP) offers an alternative approach to human lung imaging, with potential to provide similar functional information regarding pulmonary ventilation to HP-MRI.[17] Crucially, this technique uses an inert gas that can be mixed with oxygen and imaged at thermal polarization, thus avoiding the need for hyperpolarization. A small number of studies have demonstrated feasibility of this method to assess regional gas distribution in healthy volunteers[18-21] and patients with respiratory disease,[19,22-24] building on an extensive body of preclinical work.[25-32] The ability to breathe PFP over the course of several respiratory cycles offers further scope to acquire dynamic measurements of gas distribution, which has recently shown promise for evaluating airflow limitation in chronic obstructive pulmonary disease.[22,33] Nonetheless, pulmonary ^{19}F-MRI remains in relative infancy, and, to date, no studies have evaluated the utility of %VV measurements using this approach. Determining the capability of static ^{19}F-MR ventilation imaging to accurately report on such lung biomarkers in healthy volunteers is a necessary precursor to performing downstream patient studies. Moreover, the implementation of ^{19}F-MRI scan procedures at more than one study site serves to define a baseline standard for robust application of future dynamic ^{19}F-MRI protocols.

The purpose of this study was to assess the utility of static ^{19}F-MR ventilation imaging by determining the interscan and interobserver reproducibility of %VV measurements in healthy participants across two research sites.

2 | METHODS

This prospective, dual-center study was approved by the local research ethics committee (Ref 16/NE/0282) and the National Health Service Health Research Authority.

2.1 | Study population

Forty healthy participants (21 males, 19 females; ages 23-67 years, mean = 41) provided written informed consent and were screened for eligibility at one of two UK study sites (20 at Newcastle [site A]; 20 at Sheffield [site B]) between May 2018 and June 2019. Participants were recruited from local university and health care institutions at respective study sites through poster and/or email advertisement. All participants were nonsmokers in good health, with normal lung function as assessed by spirometry.[34] Study inclusion and exclusion criteria are summarized in Table 1.

2.2 | Magnetic resonance imaging

Participants underwent a single MRI scan session at one of the two study sites. All scans were performed supine using a Philips Achieva (site A) or Philips Ingenia (site B) 3T scanner (Philips Healthcare, Guildford, United Kingdom) interfaced to a ^{19}F/^{1}H chest birdcage coil (Rapid Biomedical, Rimpar, Germany). Anatomical ^{1}H scans were acquired after instructing

participants to perform a breath-hold at maximal inspiration, using a 3D spoiled gradient-echo sequence (Table 2).

Participants were subsequently instructed to inhale a 79% PFP/21% oxygen gas mixture (BOC Special Products, Guildford, United Kingdom) on five occasions during the MRI scan session (Figure 1). Each gas inhalation session lasted approximately 30 seconds, consisting of three deep breaths of gas from a starting point of relaxed end-expiration, followed by a breath-hold (13.4 seconds) at maximal inspiration. Participants were coached in the inhalation scheme before entering the MRI scanner, and instructions were reiterated before each gas inhalation session to ensure compliance with breathing maneuvers.

All gas inhalations were performed according to verbal breathing instructions provided by the attending MR radiographer. The PFP/oxygen gas mixture was administered from a 25-L reservoir bag with plastic tubing combined with a manually operated three-way gas switch, non-rebreathe valve, and mouthpiece (Hans Rudolf, Shawnee, Kansas).

An FID whole-lung spectroscopy scan (Table 2) was acquired at the onset of breath-hold during the first gas inhalation session, allowing measurement of PFP's $-CF_3$ ^{19}F resonant frequency. A 3D spoiled gradient-echo sequence (Table 2) was acquired at the onset of breath-hold for the remaining four gas inhalation sessions, enabling acquisition of four 3D ^{19}F-MR ventilation images per participant. Each ^{19}F-MRI acquisition was separated by an interval of approximately 6 minutes (mean [SD] = 358 [74] seconds), ensuring substantial gas washout from the lungs between acquisitions. Heart rate and oxygen saturations were monitored throughout using an MR-compatible pulse oximeter (Nonin Medical, Plymouth, MA). A separate supply of oxygen was available in the event of clinically significant desaturation (in which a sustained oxygen saturation below 88% would be considered an adverse event), and a clinician was present on site throughout all MRI scans.

TABLE 1 Summary of study participant eligibility criteria

Inclusion criteria	Exclusion criteria
Age 18 years or older	History of respiratory disease and/or current evidence of respiratory tract infection.
Normal spirometric function[a]	Cardiac or cerebrovascular disease, anemia, or other serious medical condition.
Body weight 50-100 kg	Current prescribed medication (excluding oral contraceptive).
	History of smoking in past 2 years: ex-smoker with greater than 2-pack year history[b] and/or ex-smoker who has smoked for more than 2 years in total.
	Contraindications to MRI (including incompatible body habitus/BMI greater than 35).
	Pregnant or breastfeeding.

Abbreviations: BMI, body mass index; FEV_1, forced expiratory volume in 1 second; FVC, forced vital capacity.

[a]FEV_1 greater than or equal to 80% predicted; FEV_1/FVC greater than or equal to 0.7.

[b]2-pack year refers to smoking 40 cigarettes per day for 1 year (1 pack = 20 cigarettes).

2.3 | Image analysis

The MR images were analyzed independently by two observers (B.P., 3 years of MRI experience; M.N., 7 years of MRI experience) using in-house software[35] developed in *MATLAB* (MathWorks, Natick MA) combined with open-source 3D segmentation functionality in *ITK-SNAP*.[36] The ^1H-MR and ^{19}F-MR image masks (depicting the anatomical boundaries of the lungs and PFP gas signal, respectively) were generated using *ITK-SNAP*'s semi-automated region-growing algorithm, allowing rigid registration of ^1H images to each of the four

TABLE 2 Summary of scan parameters for ^1H and ^{19}F MR acquisitions

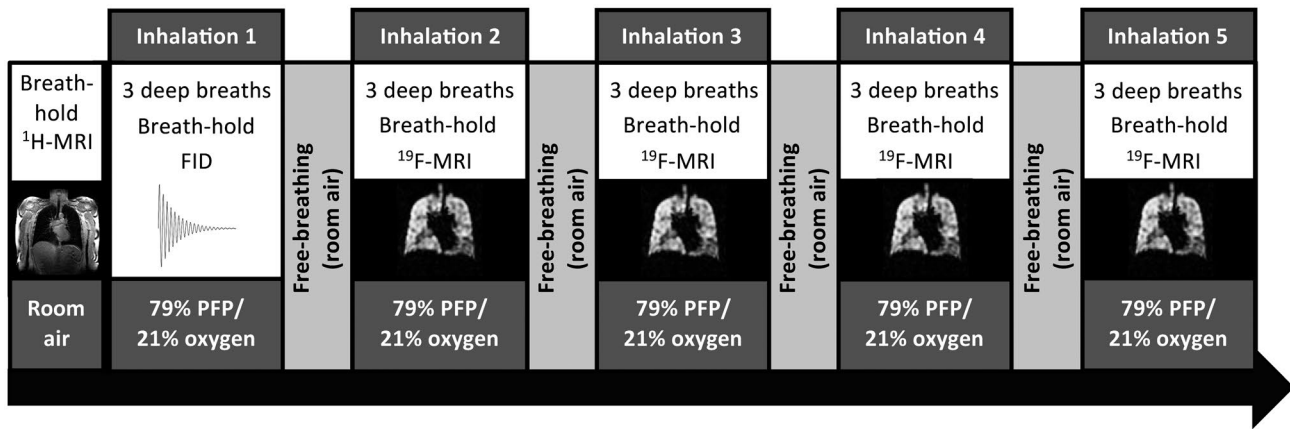| Parameter	Scan		
	^1H anatomical	^{19}F FID	^{19}F ventilation
TE (ms)	0.49	—	1.7
TR (ms)	4.0	200	7.5
Flip angle (°)	6	90	45
FOV (mm^3)	$440 \times 440 \times 247.5$	—	$400 \times (310\text{-}360) \times 250$
Resolution (mm^3)	$3 \times 3 \times 7.5$	—	$10 \times 10 \times 10$
Matrix size (voxels)	$147 \times 147 \times 33$	—	$40 \times (31\text{-}36) \times 25$
Bandwidth (Hz/pixel)	3400	—	500
Number of averages	1	50	3
Acquisition time (s)	14.6	10	13.4
Number of samples	—	256	—
Sampling frequency (Hz)	—	8000	—

FIGURE 1 Magnetic resonance imaging protocol, consisting of an initial anatomical ^{1}H-MRI breath-hold acquisition followed by five fluorine (^{19}F)-MRI breath-hold acquisitions. The first perfluoropropane (PFP) gas inhalation session was used for a whole-lung spectroscopy scan; the remaining four inhalation sessions were used to acquire ^{19}F-MR ventilation images, each separated by an interval of approximately 6 minutes
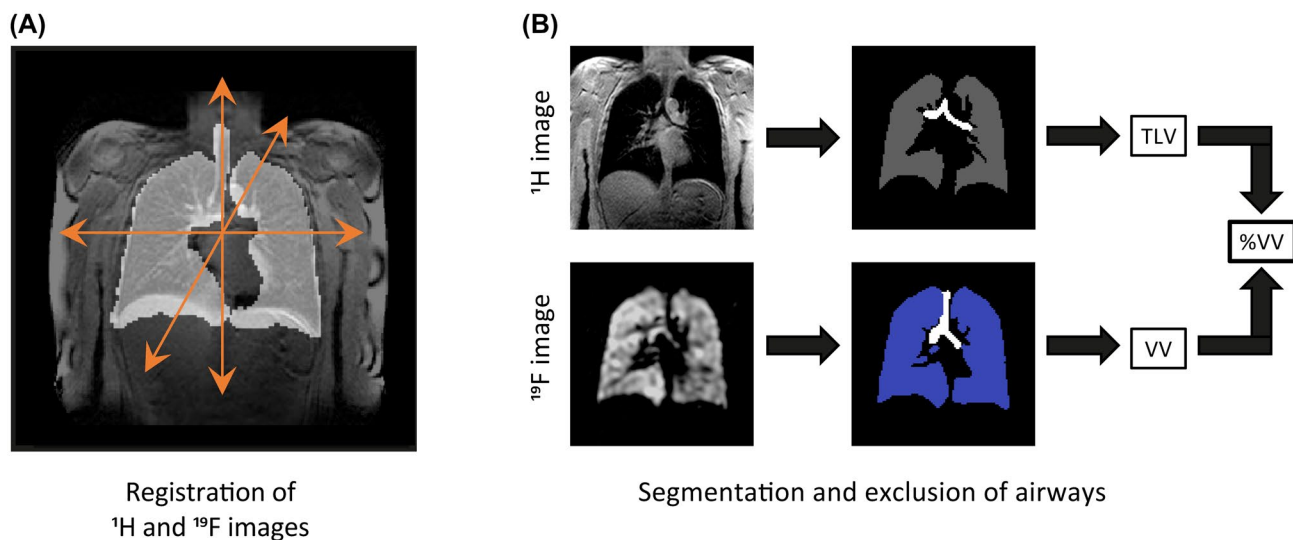

FIGURE 2 A, Registration of ^{1}H images to ^{19}F images, enabling correction of potential anatomical misalignment between scans. B, Semi-automated segmentation of individual ^{1}H and ^{19}F image slices, performed independently by two observers. The percentage ventilated lung volume (%VV) was calculated for each of the four ventilation images per participant by dividing the ventilated lung volume (VV) by the total lung volume (TLV)

corresponding ^{19}F-MR ventilation images. Registered images were subsequently segmented (Figure 2) to calculate total lung volumes (from ^{1}H images) and ventilated lung volumes for each ^{19}F-MR image, using a semi-automated approach as previously described.[35] Distinction between ventilated and nonventilated lung regions determined by the algorithm was assessed qualitatively by each observer and corrected manually where necessary, such as to amend segmentation regions where the automatic segmentation process was judged to have misassigned a region. This also included the removal of trachea, main bronchi, and major vessels from regions assigned as lung volume and ventilated lung volume. The value of %VV was subsequently calculated for each segmented image pair by dividing the ventilated volume from each ^{19}F-MR ventilation image by the total lung volume determined from the corresponding ^{1}H image.

The SNR was measured for each ventilation image by placing a 4×4 cm^2 region of interest in the apex of the right lung (signal) and a 100-cm^2 region of interest below the lung (noise) in a central image slice, where the trachea was seen to bifurcate. The SNR was calculated by applying the following expression in *MATLAB*, accounting for the Rayleigh distribution of background noise in magnitude images as follows[37]:

$$\left(\frac{\text{mean signal - mean noise}}{\text{standard deviation of noise}} \right) \sqrt{2 - \frac{\pi}{2}}.$$

2.4 | Statistical analysis

The data were analyzed by fitting linear random-effects models with three independent variance components:

differences between participants, differences between acquisitions within each participant, and differences between observers within each acquisition. This permitted an estimation of the contribution of each individual component to the total variation from the true %VV. The models were fitted in R[38] using the package lme4[39] and the lmer command (with formula = %VV ~ 1 participant/acquisition). Estimates obtained from these fits were used to compute intraclass correlation coefficients (ICCs) with confidence intervals found using the bootstrap. Coefficients of variation were computed as the SD divided by the mean over all repeated %VV measurements, expressed as a percentage. Interobserver agreement in the calculated %VV values was further evaluated using the Dice similarity coefficient as a measure of spatial overlap between segmented image pairs. Comparison of SNR and %VV measurements between the two study sites were assessed using independently sampled t-tests (95% confidence interval).

3 | RESULTS

Participant demographic information is summarized in Table 3. The ^{19}F-MRI scans were well tolerated throughout by all participants, with no adverse events. Of the 40 participants initially recruited to the study, a total of 38 were included for image analysis; 2 participants attending study site B were excluded from analysis as a result of poor compliance with breathing instructions during one or more PFP gas inhalation sessions, which affected the ability to make a true assessment of ventilated lung volumes in these participants.

3.1 | Value of %VV measurement reproducibility

Calculated %VV measurements for the remaining 38 study participants are presented in Table 4. The mean %VV value calculated for each participant was uniformly above 94% (range 94.0%-99.5%, median 98.2%).

The coefficient of variation was calculated as $CoV_{observer1}$ = 0.43% and $CoV_{observer2}$ = 0.63%. Separate analyses by the two observers revealed ICCs (95% confidence interval) of 0.683 (0.578, 0.837) for observer 1 and 0.614 (0.493, 0.784) for observer 2. The combined analysis of both observers gave components of variance for differences between participants, differences between acquisitions within each participant, and differences between observer within each acquisition of 0.90, 0.18 and 0.54, respectively. Consequently, for a given participant, the SD of the error in a single image would be $\sqrt{(0.18 + 0.54)}$ = 0.85, such that 95% of single image estimates would be within ± 1.7% of the true value.

3.2 | Interobserver agreement

Figure 3A shows coronal slices from a representative 3D ^{19}F-MRI data set from 1 healthy participant (B2: 26-year-old female; forced expiratory volume in 1 second (FEV$_1$) = 102% predicted, forced vital capacity [FVC] = 104% predicted, FEV$_1$/FVC = 83%) acquired during a 13.4-second breath-hold at maximal inspiration. Figure 3B shows orthogonal views from the same participant, with ^{19}F ventilation images (colormap) superimposed on the corresponding anatomical

TABLE 3 Summary of participant demographics

Parameter		Site A (n = 20)	Site B (n = 18)	Combined (n = 38)
Sex	Male	11	9	20
	Female	9	9	18
Age (years)	Male	35 (23-58)	43 (28-64)	39 (23-64)
	Female	43 (27-67)	42 (26-56)	43 (26-67)
	Total	39 (23-67)	43 (26-64)	41 (23-67)
Body mass index (kg/m^2)		24.4 (18.3-32.3)	23.3 (17-34.9)	23.9 (17-34.9)
Spirometry[a]	FEV$_1$ (% pred.)	105 (88-120)	100 (83-114)	103 (83-120)
	FVC (% pred.)	108 (86-125)	100 (79-117)	104 (79-125)
	FEV$_1$/FVC (%)	80 (71-93)	81 (71-96)	80 (71-96)
Mean heart rate (bpm)[b]	Pre-inhalation	70 (42-104)	65 (48-107)	68 (42-107)
	Post-inhalation	72 (44-103)	67 (48-108)	70 (44-108)
Mean oxygen saturation (%)	Pre-inhalation	98 (96-100)	98 (96-100)	98 (96-100)
	Post-inhalation	98 (95-100)	98 (93-99)	98 (93-100)

Data are presented as mean values with range in parenthesis.

[a]FEV$_1$ = forced expiratory volume in 1 second; FVC = forced vital capacity; %pred. = percentage of predicted value.

[b]bpm = beats per minute.

TABLE 4 Calculated %VV values for study participants ($N = 38$)

Participant	Observer 1					Observer 2				
	%VV 1	%VV 2	%VV 3	%VV 4	Mean %VV	%VV 1	%VV 2	%VV 3	%VV 4	Mean %VV
A1	98.0	96.9	98.6	97.4	97.7	98.9	97.2	98.9	97.8	98.2
A2	97.3	96.6	98.4	96.7	97.2	97.8	97.0	96.9	96.2	97.0
A3	98.9	98.8	98.9	98.9	98.9	98.9	98.7	97.7	98.6	98.5
A4	97.9	97.5	97.8	97.9	97.8	97.4	96.5	96.7	96.9	96.9
A5	98.6	98.2	98.8	98.8	98.6	99.7	99.2	99.1	99.1	99.2
A6	97.7	97.9	97.6	98.2	97.8	97.5	97.4	97.3	98.9	97.8
A7	98.8	99.1	98.5	98.3	98.7	98.6	98.3	98.9	97.9	98.4
A8	98.2	98.0	97.5	98.7	98.1	98.9	99.6	98.8	99.1	99.1
A9	98.1	97.8	97.7	98.1	97.9	97.9	97.4	97.1	98.1	97.6
A10	98.3	98.6	98.8	98.8	98.6	99.3	99.1	99.5	99.3	99.3
A11	97.8	97.8	98.1	98.5	98.1	97.8	97.4	98.0	97.7	97.7
A12	98.5	98.6	98.9	99.0	98.7	99.0	98.9	98.6	98.8	98.8
A13	98.5	98.7	99.1	98.9	98.8	98.9	99.2	99.0	98.9	99.0
A14	98.8	98.9	98.7	99.0	98.9	99.4	99.6	99.6	99.3	99.5
A15	97.6	97.8	98.3	98.3	98.0	97.7	97.9	97.9	97.6	97.8
A16	99.2	99.3	99.4	99.2	99.3	99.4	99.2	99.2	99.1	99.2
A17	98.9	98.9	99.1	99.1	99.0	98.3	98.5	97.3	98.4	98.1
A18	97.9	97.6	97.9	97.5	97.7	98.6	97.6	97.7	97.3	97.8
A19	98.7	97.3	97.8	99.2	98.3	97.8	96.4	97.6	97.7	97.4
A20	99.1	99.3	99.3	98.7	99.1	97.3	98.6	98.2	98.3	98.1
B1	96.4	96.6	96.3	95.4	96.2	94.3	94.1	96.1	97.1	95.4
B2	99.8	99.1	99.1	99.2	99.3	99.5	99.5	99.6	99.5	99.5
B3	98.1	98.5	98.2	98.5	98.3	97.6	98.3	97.6	97.2	97.7
B4	97.0	96.6	97.6	96.3	96.9	96.6	95.9	97.2	95.5	96.3
B5	98.4	98.1	98.4	98.7	98.4	98.2	97.6	98.2	97.8	97.9
B6	98.3	98.4	97.8	97.7	98.0	98.3	96.9	97.5	97.9	97.7
B7	99.4	99.2	99.6	99.8	99.5	98.5	98.5	98.3	98.9	98.5
B8	99.4	99.2	99.3	99.2	99.3	97.1	98.7	98.4	97.6	97.9
B9	99.3	98.4	99.0	97.6	98.6	96.9	97.0	96.1	96.4	96.6
B10	99.3	99.1	99.1	99.4	99.2	99.0	98.2	98.6	98.2	98.5
B11	98.0	98.0	97.7	98.0	97.9	97.6	97.2	97.2	97.3	97.3
B12	98.9	98.8	99.1	99.2	99.0	98.7	97.3	98.6	97.8	98.1
B13	93.8	97.3	97.0	98.4	96.6	90.4	93.2	95.3	96.9	94.0
B14	97.8	97.6	93.6	95.3	96.1	96.3	97.8	90.2	95.8	95.0
B15	97.6	98.7	99.1	98.9	98.5	98.1	98.7	98.0	99.0	98.4
B16	98.9	99.1	98.9	99.0	99.0	98.9	97.7	98.1	98.4	98.3
B17	99.3	99.4	99.4	99.2	99.3	98.2	97.7	98.3	98.6	98.2
B18	96.1	95.7	95.4	97.1	96.1	98.6	97.3	95.6	97.2	97.2

[1]H MR images (grayscale). Homogeneous gas distribution can be visualized throughout the entire lung fields, with only minor apparent ventilation heterogeneity observed toward the most peripheral anterior–posterior lung slices.

The mean (SD) calculated %VV values across all analyzed participant data sets ($N = 38$) were similar between observers (98.2 [0.9]% and 97.8 [1.2]% for observer 1 and observer 2, respectively). The random effects model estimated the variation about the true %VV value due to observer variation as 0.54.

Figure 4A shows a comparison of ^{19}F-MR image segmentations performed by the two observers for 1 participant (A7: 37-year-old male; $FEV_1 = 113\%$ predicted, FVC = 120%
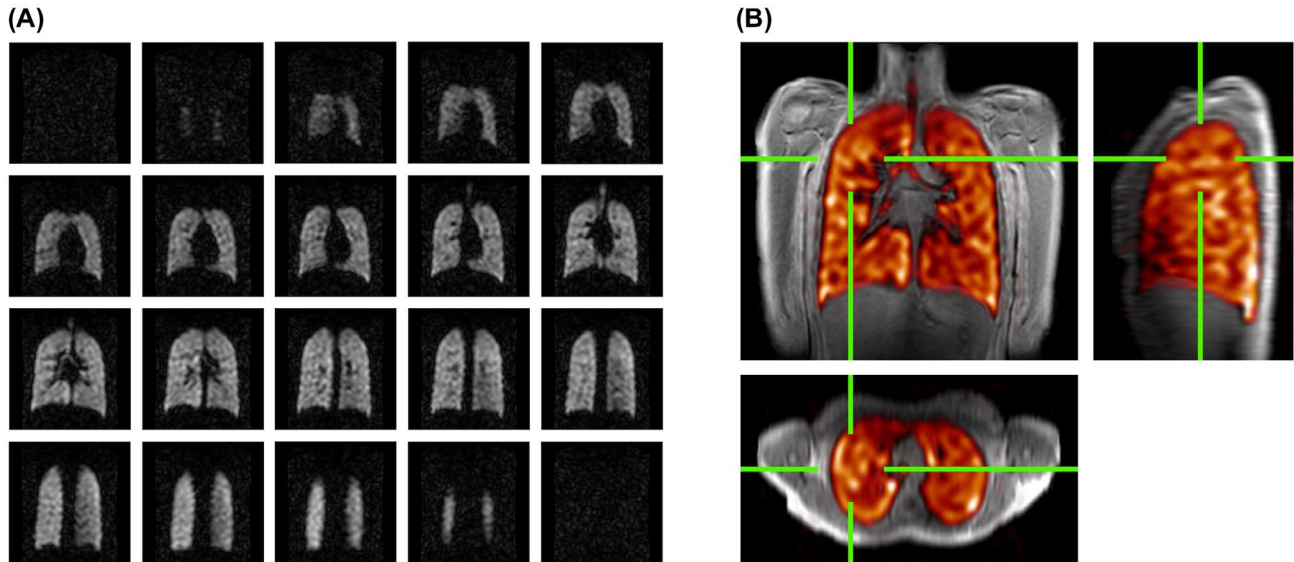
FIGURE 3 A, Representative ^{19}F-MR ventilation images (coronal views) from a healthy participant, acquired during a 13.4-second breath-hold scan following three deep breaths of a 79% PFP/21% oxygen gas mixture. The original magnitude image is displayed without any image processing or thresholding applied. An SNR of 13.5 was measured in a central lung slice of this image. B, Combined ^{1}H and ^{19}F-MR ventilation images (colored, orthogonal views) in the same participant, showing homogeneous gas distribution throughout the lung fields
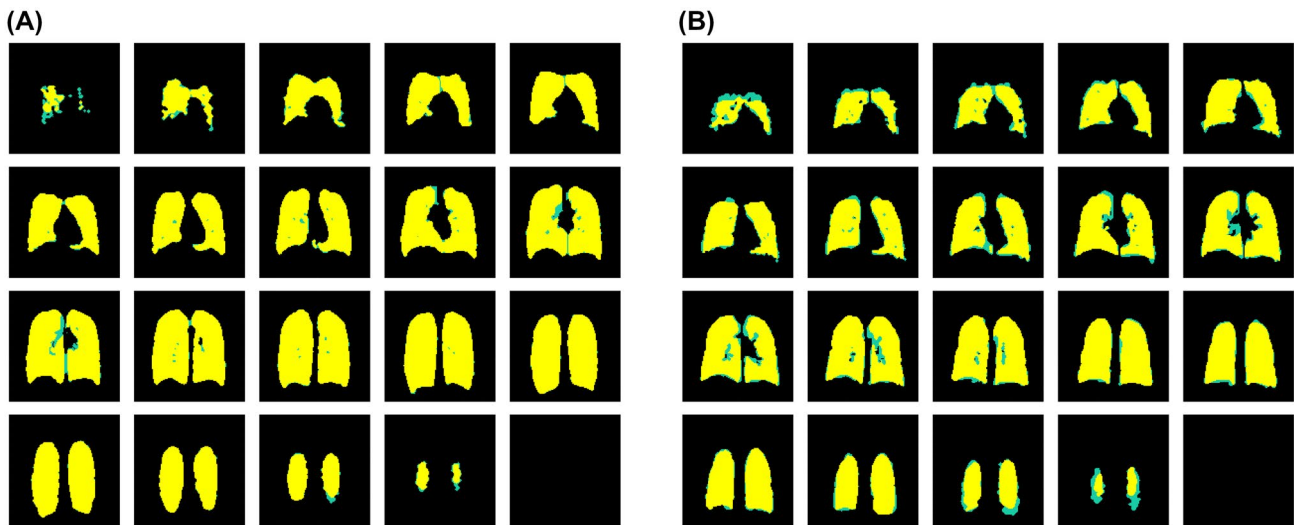

FIGURE 4 Combined ^{19}F image segmentations performed independently by two observers, showing agreement (yellow) and disagreement (green) between respective segmentations. A, Example of close agreement in segmentations performed by the two observers (Dice similarity coefficient = 0.98), in which discrepancy is confined primarily toward the anterior slices. B, Example of greater discrepancy in segmentations performed by the two observers (Dice similarity coefficient = 0.93), in which more widespread differences are visible

predicted, $FEV_1/FVC = 76\%$). Interobserver agreement for respective image segmentations is shown in yellow, while disagreement between observers is shown in green. There is a high degree of spatial overlap between individual observer segmentations, with disagreement most prominent toward the peripheral lung slices. Figure 4B shows an equivalent combined segmentation data set from a different participant (A6: 34-year-old male; $FEV_1 = 113\%$ predicted, FVC = 118% predicted, $FEV_1/FVC = 79\%$), in whom the discrepancy between observer segmentations (green) is more apparent. The Dice

similarity coefficient, calculated as a measure of interobserver agreement across all ^{19}F-MR image segmentations performed, demonstrated a high mean (SD) value of 0.97 (0.02).

3.3 | Comparison between sites

Image quality was of a sufficient standard across the two study sites to determine %VV values using the semi-automated segmentation software, with comparable SNR achieved between

the respective study sites (mean SNR_{SiteA} = 14.8 [2.5]; range = 8.4-19.8; mean SNR_{SiteB} = 13.9 [4.0]; range = 6.5-25.4). An independently sampled t-test revealed no evidence of a difference in SNR values between study sites (P = .11).

The %VV measurements, averaged across both observers to provide a single value per participant, were compared between the two study sites. An independently sampled t-test found no evidence of a difference in %VV values between the two study sites (P = .09), in which the mean %VV was 98.3 (0.6)% (range = 97.1-99.3%) for site A, and 97.7 (1.3)% (range = 95.3-99.4%) for site B, respectively.

3.4 | Intraparticipant agreement

The SD around the mean of the four within-participant %VV measurements were $mean_{observer1}$ = 98.2% (SD = 0.4, range = 0.0-1.7) and $mean_{observer2}$ = 97.8% (SD = 0.5, range = 0.0-2.9), measured by observers 1 and 2, respectively.

The spread of the four intraparticipant SNR measurements around the mean value were mean SNR_{SiteA} = 14.8 (SD = 1.2, range = 0.4-2.3) and mean SNR_{SiteB} = 13.9 (SD = 1.2, range = 0.3-2.5).

4 | DISCUSSION AND CONCLUSIONS

This study investigated the ability of ^{19}F-MRI of inhaled PFP to provide quantitative measures of pulmonary ventilation, demonstrating good same-day reproducibility of %VV measurements in a cohort of healthy participants. This work builds on a growing literature base surrounding the use of PFP as a potentially viable alternative to HP-MRI for human ventilation imaging.

A goal of this study was to establish the technical feasibility of performing ^{19}F-MR ventilation imaging across different study sites, while maintaining reproducibility of data acquisition. We have successfully implemented a ^{19}F-MR imaging protocol to acquire ventilation images from 38 healthy participants at two research centers with sufficient image quality and SNR to determine %VV measurements. The %VV and its counterpart, ventilation defect percentage (equal to 100% minus %VV), are well-established metrics within the HP-MRI literature, providing quantitative volume-independent measures that are sensitive to pathology and therapeutic response.[7,8] Our findings indicate a high degree of consistency in calculated %VV values across all study participants, with a low coefficient of variation between respective ^{19}F-MR acquisitions. It should be noted, however, that statistical assessment of %VV values in a cohort of healthy participants will inevitably be skewed toward the upper end of the %VV scale

(and ventilation defect percentage calculations from the data would be equivalently biased).

The ICCs we report are slightly lower than values previously published for [129]Xe and [3]He.[7,9,11] However, ICCs are determined by the values of the between-acquisition and between-observer components of variance relative to the between-participant component of variance. There was little variation in %VV values measured in our cohort of healthy participants compared with previously reported studies,[7,9] with most of our participants demonstrating %VV values between 97% and 99%. As such, the relatively modest ICC values observed in our study likely reflect the marked homogeneity of our particular cohort, rather than diminished reproducibility per se. The similarity of within-participant %VV values between observers (98.2% and 97.8% for observer 1 and 2, respectively), and the small intra-participant SDs around these values (0.4 and 0.5, respectively), support the reproducibility of this technique. Moreover, the high degree of interobserver consistency and precision in calculated %VV values adds weight to the ability of our approach to provide reliable measures of pulmonary ventilation in a large group of healthy participants. Downstream application of these methods in patient cohorts will be beneficial in determining the capability of ^{19}F-MRI across a broader spectrum of ventilation defect severities.

Formal evaluation of the safety of inhaled PFP (eg, through a clinical trial of an investigational medicinal product) was beyond the scope of this study. Nonetheless, our work adds weight to the growing body of evidence surrounding the use of PFP for human ventilation imaging.[18,19,22] To the best of our knowledge, this is the largest reported study to date involving ^{19}F-MRI of inhaled PFP. In total, 200 ^{19}F-MRI scans were performed on the 40 participants recruited to the study. Each acquisition consisted of three deep breaths of a 79% PFP/21% oxygen gas mixture. We observed no adverse events relating to gas inhalation, with no effect on participant heart rate or oxygen saturation (summarized in Table 3). This has implications for performing larger clinical studies, including future multicenter trials involving patients with respiratory disease, which will be crucial in establishing suitability of this approach for wider clinical use.

There were some limitations to our study. Notably, 2 participants were excluded from image analysis due to poor compliance with breathing instructions, which affected the quality of acquired ventilation images. In both of these cases, at least one of the four gas inhalation sessions was characterized by a failure to achieve maximal inspiration, which did not comply with the coached protocol. This resulted in images with a dearth of signal in combination with a substantial reduction in measured lung volume. Adherence to correct breathing instructions is crucial to maintaining reproducibility of image acquisitions.

Importantly, our PFP inhalation protocol differs with HP-MRI ventilation imaging, which typically involves a single inhalation of a small, fixed volume of gas. The sensitivity of inhaled PFP to changes in lung inflation level has previously been reported[40] and underpins the specific breathing protocol used in this study (ie, three deep wash-in breaths of gas, followed by a breath-hold at maximum inspiration). This contrasts with the inhalation protocol reported by Couch et al, who used relaxed tidal wash-in breaths, up to a cumulative 5 L, followed by a fixed (1 L) inhalation and breath hold.[18] Nonetheless, by adopting this approach, the PFP wash-in volume may be standardized relative to the volume of maximal inhalation achievable by each participant, rather than adopting a fixed wash-in volume regardless of lung capacity. Our breathing protocol was therefore developed to achieve substantial replacement of air by PFP within the lungs, maximizing the SNR in ventilated regions and facilitating reproducibility of scan acquisitions. At the same time, the brevity of this wash-in breathing protocol was designed to preserve the discernibility of poorly ventilated lung regions that is characteristic of patients with obstructive airways disease (data from pilot and ongoing studies not shown). Importantly, in the 38 participants who performed breathing maneuvers as instructed, we demonstrated good reproducibility of %VV measurements.

The use of advanced MR coil hardware (eg, array coils)[41] may help to improve the overall SNR of ^{19}F-MR images, as well as address the spread of SNR values observed between participants. This may, in part, stem from differences in coil loading associated with varying body habitus, in addition to differences in breathing efficacy relating to the gas wash-in protocol. Moreover, improved coil design may mitigate the tendency for spatially variable signal inhomogeneities (with slight signal dropoff particularly apparent toward the outermost anterior slices). Although this potentially reflects a degree of physiological ventilation heterogeneity, it is more likely the result of local field inhomogeneity arising from coil–scanner interaction. Segmentation of these particular slices does not, however, appear to have a substantial effect on global %VV measurements.

The ability to breathe PFP continuously over several respiratory cycles has recently been used as an alternative to static breath-hold imaging,[22] enabling dynamic image acquisition during free breathing. This approach plays to the strengths of ^{19}F-MRI of PFP compared with HP-MRI, in which the thermally polarized gas does not exhibit the irrecoverable loss of signal over a dynamic imaging series that is unavoidable with hyperpolarized tracer gases (ie, ^{3}He and ^{129}Xe). Dynamic imaging reduces the requirement to follow a rigid inhalation protocol and offers potential advantages for imaging of patients with respiratory disease or younger children who may not be able to tolerate breath-hold maneuvers. The repeatability of dynamic gas wash-out measurements in patients with chronic obstructive pulmonary disease has recently been reported.[33] Nonetheless, given the widespread use of %VV measurements in HP-MRI literature, our study provides an important benchmark from which to determine the utility of static ^{19}F-MR ventilation imaging in preparation for performing future patient studies.

We report for the first time an evaluation of %VV measurements acquired by ^{19}F-MRI of inhaled PFP, demonstrating good same-day reproducibility in a large number of healthy participants. The successful implementation of scan procedures across two different study sites provides a firm foundation from which to compare image quality and variability in patients with respiratory disease, including application to dynamic ventilation imaging.

ORCID
Mary A. Neal https://orcid.org/0000-0002-5634-7586
Adam M. Maunder https://orcid.org/0000-0002-1161-8741
A. John Simpson https://orcid.org/0000-0003-4731-7294
Jim M. Wild https://orcid.org/0000-0002-7246-8660
Peter E. Thelwall https://orcid.org/0000-0003-1795-6394

REFERENCES
1. Wild JM, Marshall H, Bock M, et al. MRI of the lung (1/3): methods. *Insights Imaging*. 2012;3:345-353.
2. Fain S, Schiebler ML, McCormack DG, Parraga G. Imaging of lung function using hyperpolarized helium-3 magnetic resonance imaging: review of current and emerging translational methods and applications. *J Magn Reson Imaging*. 2010;32:1398-1408.
3. Mugler JP, Altes TA. Hyperpolarized ^{129}Xe MRI of the human lung. *J Magn Reson Imaging*. 2013;37:313-331.
4. Hamedani H, Clapp JT, Kadlecek SJ, et al. Regional fractional ventilation by using multibreath wash-in ^{3}He MR imaging. *Radiology*. 2016;279:917-924.
5. Virgincar RS, Cleveland ZI, Kaushik SS, et al. Quantitative analysis of hyperpolarized ^{129}Xe ventilation imaging in healthy volunteers and subjects with chronic obstructive pulmonary disease. *NMR Biomed*. 2013;26:424-435.
6. Ouriadov A, Farag A, Kirby M, McCormacck DG, Parraga G, Santyr GE. Lung morphometry using hyperpolarized ^{129}Xe apparent diffusion coefficient anisotropy in chronic obstructive pulmonary disease. *Magn Reson Med*. 2013;70:1699-1706.
7. Horn FC, Tahir BA, Stewart NJ, et al. Lung ventilation volumetry with same-breath acquisition of hyperpolarized gas and proton MRI. *NMR Biomed*. 2014;27:1461-1467.
8. Mathew L, Wheatley A, Castillo R, et al. Hyperpolarized ^{3}He magnetic resonance imaging. Comparison with four-dimensional x-ray computed tomography imaging in lung cancer. *Acad Radiol*. 2012;19:1546-1553.

9. Ebner L, He MU, Virgincar RS, et al. Hyperpolarized [129]Xenon magnetic resonance imaging to quantify regional ventilation differences in mild to moderate asthma: a prospective comparison between semiautomated ventilation defect percentage calculation and pulmonary function tests. *Invest Radiol*. 2017;52:120-127.

10. Kirby M, Svenningsen S, Owrangi A, et al. Hyperpolarized [3]He and [129]Xe MR imaging in healthy volunteers and patients with chronic obstructive pulmonary disease. *Radiology*. 2012;265:600-610.

11. Mathew L, Evans A, Ouriadov A, et al. Hyperpolarized [3]He magnetic resonance imaging of chronic obstructive pulmonary disease. Reproducibility at 3.0 Tesla. *Acad Radiol*. 2008;15:1298-1311.

12. Kirby M, Heydarian M, Svenningsen S, et al. Hyperpolarized [3]He magnetic resonance functional imaging semiautomated segmentation. *Acad Radiol*. 2012;19:141-152.

13. Stewart NJ, Chan HF, Hughes PJC, et al. Comparison of [3]He and [129]Xe MRI for evaluation of lung microstructure and ventilation at 1.5T. *J Magn Reson Imaging*. 2018;48:632-642.

14. O'Sullivan B, Couch M, Roche JP, et al. Assessment of repeatability of hyperpolarized gas MR ventilation functional imaging in cystic fibrosis. *Acad Radiol*. 2014;21:1524-1529.

15. Pike D, Kirby M, Guo F, McCormack DG, Parraga G. Ventilation heterogeneity in ex-smokers without airflow limitation. *Acad Radiol*. 2015;22:1068-1078.

16. Svenningsen S, Nair P, Guo F, McCormack DG, Parraga G. Is ventilation heterogeneity related to asthma control? *Eur Respir J*. 2016;48:370-379.

17. Couch MJ, Ball IK, Li T, Fox MS, Biman D, Albert MS. [19]F MRI of the lungs using inert fluorinated gases: challenges and new developments. *J Magn Reson Imaging*. 2019;49:343-354.

18. Couch MJ, Ball IK, Li T, et al. Pulmonary ultrashort echo time ^{19}F MR imaging with inhaled fluorinated gas mixtures in healthy volunteers: feasibility. *Radiology*. 2013;269:903-909.

19. Halaweish AF, Moon RE, Foster WM, et al. Perfluoropropane gas as a magnetic resonance lung imaging contrast agent in humans. *Chest*. 2013;144:1300-1310.

20. Neal MA, Pippard BJ, Hollingsworth KG, et al. Optimized and accelerated ^{19}F-MRI of inhaled perfluoropropane to assess regional pulmonary ventilation. *Magn Reson Med*. 2019;82:1301-1311.

21. Neal MA, Pippard BJ, Maunder A, et al. 19F-MRI of inhaled perfluoropropane for assessment of pulmonary ventilation: a multi-centre reproducibility study in healthy volunteers. In: Proceedings of the 28th Annual Meeting of ISMRM, Online Virtual Conference, 2020. Abstract 440.

22. Gutberlet M, Kaireit TF, Voskrebenzev A, et al. Free-breathing dynamic ^{19}F gas MR imaging for mapping of regional lung ventilation in patients with COPD. *Radiology*. 2018;286:1040-1051.

23. Pippard B, Neal M, Maunder A, et al. Assessing regional lung ventilation with ^{19}F-MRI of inhaled perfluoropropane. *Eur Respir J*. 2018;52:OA3799.

24. Goralski JL, Chung SH, Glass TM, et al. Dynamic perfluorinated gas MRI reveals abnormal ventilation despite normal FEV1 in cystic fibrosis. *JCI Insight*. 2020;5:e133400.

25. Pérez-Sánchez JM, Pérez De Alejo R, Rodríguez I, Cortijo M, Peces-Barba G, Ruiz-Cabello J. In vivo diffusion weighted ^{19}F MRI using SF$_6$. *Magn Reson Med*. 2005;54:460-463.

26. Ouriadov AV, Fox MS, Couch MJ, Li T, Ball IK, Albert MS. In vivo regional ventilation mapping using fluorinated gas MRI with an x-centric FGRE method. *Magn Reson Med*. 2015;74:550-557.

27. Wolf U, Scholz A, Heussel CP, Markstaller K, Schreiber WG. Subsecond fluorine-19 MRI of the lung. *Magn Reson Med*. 2006;55:948-951.

28. Schreiber WG, Eberle B, Laukemper-Ostendorf S, et al. Dynamic ^{19}F-MRI of pulmonary ventilation using sulfur hexafluoride (SF$_6$) gas. *Magn Reson Med*. 2001;45:605-613.

29. Adolphi NL, Kuethe DO. Quantitative mapping of ventilation-perfusion ratios in lungs by ^{19}F MR imaging of T$_1$ of inert fluorinated gases. *Magn Reson Med*. 2008;59:739-746.

30. Keuthe DO, Filipzak PT, Hix JM, et al. Magnetic resonance imaging provides sensitive in vivo assessment of experimental ventilator-induced lung injury. *Am J Physiol Lung Cell Mol Physiol*. 2016;331:L208-L218.

31. Couch MJ, Fox MS, Viel C, et al. Fractional ventilation mapping using inert fluorinated gas MRI in rat models of inflammation and fibrosis. *NMR Biomed*. 2016;29:545-552.

32. Ebner B, Behm P, Jacoby C, et al. Early assessment of pulmonary inflammation by ^{19}F MRI in vivo. *Circ Cardiovasc Imaging*. 2010;3:202-210.

33. Gutberlet M, Kaireit TF, Voskrebenzev A, et al. Repeatability of regional lung ventilation quantification using fluorinated (^{19}F) gas magnetic resonance imaging. *Acad Radiol*. 2019;26:395-403.

34. Miller MR, Hankinson J, Brusasco V, et al. Standardisation of spirometry. *Eur Respir J*. 2005;26:319-338.

35. Hughes PJC, Horn FC, Collier GJ, Biancardi A, Marshall H, Wild JM. Spatial fuzzy c-means thresholding for semiautomated calculation of percentage lung ventilated volume from hyperpolarized gas and ^{1}H MRI. *J Magn Reson Imaging*. 2018;47:640-646.

36. Yushkevich PA, Piven J, Hazlett HC, et al. User-guided 3D active contour segmentation of anatomical structures: significantly improved efficiency and reliability. *Neuroimage*. 2006;31:1116-1128.

37. Edelstein W, Bottomley P, Pfeifer L. A signal-to-noise calibration procedure for NMR imaging systems. *Med Phys*. 1984;11:180-185.

38. R Core Team. *R: A Language and Environment for Statistical Computing*. 2015. https://www.R-project.org/. Accessed September 14, 2020.

39. Bates D, Maechler M, Bolker B, et al. *lme4: Linear Mixed-Effects Models using Eigen and S4*. R package version 1.1-7. 2014. Available at http://CRAN.R-project.org/package=lme4. Accessed September 14, 2020.

40. Maunder A, Rao M, Robb F, Wild JM. Optimization of steady-state free precession MRI for lung ventilation imaging with [19]F C$_3$F$_8$ at 1.5T and 3T. *Magn Reson Med*. 2019;81:1130-1142.

41. Maunder A, Rao M, Robb F, Wild JM. An 8-element Tx/Rx array utilizing MEMS detuning combined with 6 Rx loops for ^{19}F and ^{1}H lung imaging at 1.5T. *Magn Reson Med*. 2020;84:2262-2277.